Self-consistent calculations of the energy bands and bonding properties of $B_{12}C_3$

D. M. Bylander, Leonard Kleinman, and Seongbok Lee
Department of Physics, University of Texas, Austin, Texas 78712
(Received 12 January 1990)

Using a basis set of ~3580 plane waves, we perform *ab initio* self-consistent calculations of the energy bands and cohesive energy of $B_{12}C_3$. Calculating stresses and forces, both the lattice constants and the positions of the atoms in the unit cell are determined. If trigonal symmetry is forced (i.e., all three carbons on the chain), the cohesive energy is 108.20 eV/(unit cell). In the experimentally observed structure with one boron on each chain and one carbon on each icosahedron, the cohesive energy is 109.48 eV/(unit cell). An indirect energy gap of 2.781 eV is obtained for this structure and charge-density–contour plots indicate that the ratio of the charge on the carbons to that on the borons is much greater than the 4:3 ratio of their valences.

I. INTRODUCTION

Because of its propensity to form icosahedra whose fivefold rotational symmetry is not compatible with translational symmetry, boron together with its compounds forms a huge number of structures, many of which have very large unit cells. For example, elemental boron crystallizes[1] in two rhombohedral polymorphs, B_{12} and B_{105}, as well as tetragonal B_{50}. Of the plethora of compounds boron forms, the carbides are perhaps the most interesting. Both B_{105} and $B_{12}C_3$ are stronger than steel, harder than corundum,[2(a)] lighter than aluminum; the carbide is used in armor. Because of their high melting temperature, anomalously large Seebeck coefficients, and low thermal conductivity, the carbides' use as a very high-temperature thermoelectric material has been suggested.[3]

Boron carbide is scientifically fascinating. The $B_{12}C_3$ structure with its $B_{11}C$ icosahedra and CBC chains is shown in Fig. 1. However, the carbon content may be reduced from 20% down to 8.8% and the structure remains stable with B atoms replacing C's. How this structure can accommodate such a large range of carbon compositions without having any interstitial atoms is not understood.[4] Although there is general agreement concerning the $B_{12}C_3$ structure, there is no agreement as to whether the icosahedral carbon or one of the chain carbons is replaced by boron in the $B_{13}C_2$ structure. X-ray data indicate it is the former,[4,5] whereas Emin and coworkers, citing electrical and thermal transport measurements[6] and Raman spectra[7] and a theoretical analysis of the free energy[3] favor the latter. Furthermore, the boron icosahedron has been shown[8] to have 13 intraicosahedral bonding orbitals plus 12 outward-pointing bonding orbitals. Since B_{12} has 36 $2s$ and $2p$ electrons, this leaves the icosahedra two electrons short of completing all their bonds and it has been suggested[8] that the icosahedra should be negatively doubly ionized in $B_{13}C_2$. Yet the x-ray data show no excess charge on the icosahedra.[5]

There have heretofore been at least two electronic-structure calculations of $B_{12}C_3$ but none which could be called *ab initio*. Both expanded in a single $2s$ and $2p$ orbital on each site. One[9] calculated the potential from a superposition of atomic charges and the other[10] used a "universal form" for the matrix elements. The former calculated only B_{12}(CCC) whereas the latter compared B_{12}(CCC) with $B_{11}C$(CBC). Our calculations are performed using the factorized form[11] of norm-conserving pseudopotentials which are chosen to yield pseudo-wavefunctions whose first *and* second energy derivatives of their logarithmic derivatives are identical to those of the true eigenfunctions.[12,13] We used Kohn-Sham[14] exchange and Wigner[15] correlation and expand in between 3570 and 3593 plane waves at 32 points in the Brillouin zone (BZ). Since the BZ's here have less than $\frac{1}{9}$th the volume of the diamond BZ, this sample is comparable to the standard 256-point sample in the diamond BZ (also known as the "special" ten **k**-point sample[16] of the irreducible wedge of the diamond BZ). In the next section, after reporting on our total energy and Hellman-Feynman calculations for the lattice constants and positions of the atoms within the unit cell, and finding, as expected, that $B_{11}C$(CBC) is the ground-state configuration, we plot its energy bands and contours of constant charge density both in the reflection plane containing the CBC chain and over the 12 independent faces of the icosahedron. This, as well as the nature of individual electronic states near the energy gap, leads us to some conclusions concerning the nature of the bonding in $B_{12}C_3$. In a future paper we shall attempt to settle the controversy concerning the ground-state configuration of $B_{13}C_2$. In appendices to this paper we give some details of how the very large plane-wave-basis-set calculations are performed.

II. RESULTS

Figure 1 is a photograph of a model of the $B_{12}C_3$ crystal in which we have labeled the centers of the icosahedra with Greek letters, the icosahedral atoms with lower case Roman, and the chain atoms with upper case Roman. For B_{12}(CCC), which has threefold symmetry about the

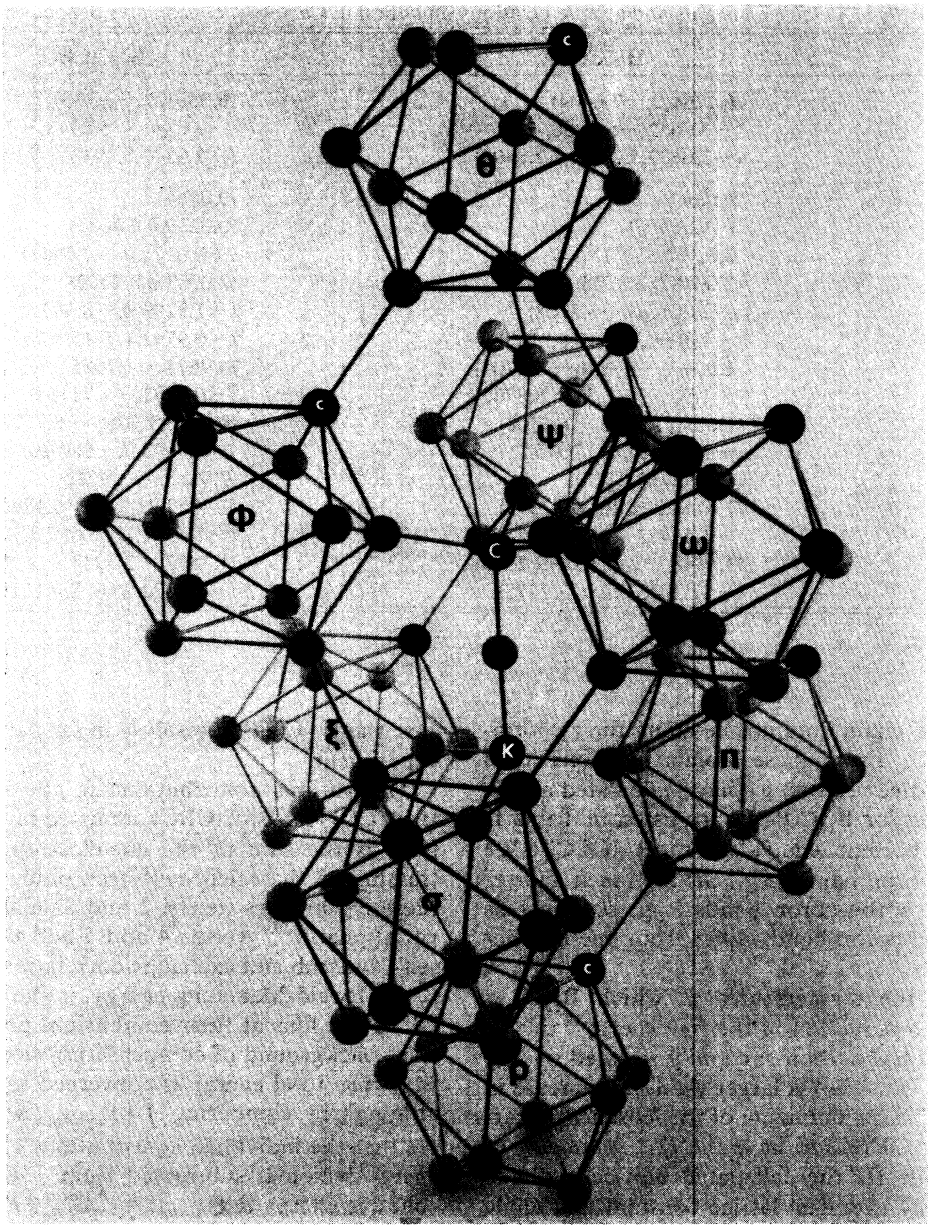

FIG. 1. Photograph of a $B_{11}C(CBC)$ crystal model, atoms c, C, and K are carbon and the rest are boron. Various lattice points in the middles of the icosahedra are labeled with Greek letters.

$\theta\rho$ axis, it contains an $ABCA$ array of hexagonal planes of icosahedra. θ and ρ are in A planes, B contains the triangle $\varphi\psi\omega$, and C the triangle $\xi\pi\sigma$. The primitive lattice vectors are $\theta\varphi$, $\theta\psi$, and $\theta\omega$. If the angles between these primitive vectors were 60°, $B_{12}(CCC)$ would be a fcc array of B_{12} icosahedra with CCC chains which lie along the (111) direction and which are centered at the octahedral interstitial site. $\overline{\theta\psi}$ may be replaced by $\overline{\theta\pi}=\overline{\theta\psi}+\overline{\theta\omega}$. This has the advantage that the parallelogram $\theta\pi\rho\varphi$ is a reflection plane even in $B_{11}C(CBC)$. This plane contains the long chain of atoms beginning with d and z in θ to c and w in φ then the (CBK) chain to d and z in π and finally c and w in ρ. A $\theta\pi$ translation connects the last four atoms in the chain to the first four. A system with only one reflection plane (C_{1h} symmetry) is known to crystallize in a monoclinic lattice.[17] The vector $\overline{\theta\omega}-\overline{\theta\psi}$ is perpendicular to the parallelogram and represents a nonprimitive lattice vector for the face-centered monoclinic lattice (only one of the two rectangular pairs of faces is centered). We define a Cartesian set of coordinates with the y axis along $\overline{\theta\omega}-\overline{\theta\psi}$, the z axis along $-(\overline{\theta\pi}+\overline{\theta\varphi})$, and the x axis perpendicular to both. In Table I we list the calculated $\overline{\theta\varphi}$, $\overline{\theta\psi}$, and $\overline{\theta\omega}$ in terms of these Cartesian coordinates for both $B_{12}(CCC)$ and $B_{11}C(CBC)$. In addition, with atom B taken as the origin we list the calculated positions of all the atoms, taking atoms x, y, and z in θ, a, b, and c in ρ, and the remaining icosahedral atoms to be those that bond with C or K.

TABLE I. Lattice constants and atomic positions (in bohrs) in Cartesian coordinates defined in text.

	B_{12}(CCC)	$B_{11}C$(CBC)
$\overline{\theta\phi}$	(6.1264,0,−7.6404)	(6.0681,0,−7.3964)
$\overline{\theta\psi}$	(−3.0632,−5.3056,−7.6404)	(−3.0341,−5.2948,−7.6598)
$\overline{\theta\omega}$	(−3.0632,5.3056,−7.6404)	(−3.0341,5.2948,−7.6598)
B	(0,0,0)	(0,0,0)
C	(0,0,2.5507)	(0.0219,0,2.7035)
K	(0,0,−2.5507)	(−0.0171,0,−2.7441)
z	(2.0018,0,8.8708)	(2.0087,0,8.7232)
c	(−2.0018,0,−8.8708)	(−1.9299,0,−8.9411)
x	(−1.0090,1.7336,8.8708)	(−0.9792,1.7115,8.7178)
b	(1.0090,−1.7336,−8.8708)	(0.9673,−1.7085,−8.7724)
y	(−1.0090,−1.7336,8.8708)	(−0.9792,−1.7115,8.7178)
a	(1.0090,1.7336,−8.8708)	(0.9673,1.7085,−8.7724)
d	(−3.0295,0,−3.2375)	(−2.9802,0,−3.3620)
w	(3.0295,0,3.2375)	(2.9665,0,3.2904)
g	(1.5148,2.6236,−3.2375)	(1.4853,2.5943,−3.1899)
k	(−1.5148,−2.6236,3.2375)	(−1.4802,−2.6027,3.1219)
h	(1.5148,−2.6236,−3.2375)	(1.4853,−2.5943,−3.1899)
v	(−1.5148,2.6236,3.2375)	(−1.4802,2.6027,3.1219)

Note that the *CBK* chain does not lie along the z coordinate in $B_{11}C$(CBC). From these atomic positions (mod the appropriate lattice vectors) we have calculated all the bond lengths; those for $B_{11}C$(BCB) are listed in Table II in groups which become equivalent in B_{12}(CCC). We note that carbon-boron bonds (e.g., *ch*) are much shorter than "equivalent" boron-boron bonds (e.g., *zk*) whereas "equivalent" boron-boron bonds differ from one another by smaller amounts.

Apparently, at the temperatures at which $B_{12}C_3$ is made, the $-kT\ln 6$ reduction in the free energy[18] due to having the icosahedral carbon randomly situated on one of the a, b, c, x, y, or z sites is larger than the increase in internal energy. This randomizing of the icosahedral carbon site causes $B_{11}C$(CBC) to have the D_{3d} symmetry of B_{12}(CCC). In Table III the calculated unit-cell volume and rhombohedrally averaged lattice constant and angle as well as averaged bond lengths of $B_{11}C$(CBC) are compared with those calculated for B_{12}(CCC) and with experiment.[4] The calculated lattice constant is too small by 0.44%, which is typical for local-density-approximation[14] (LDA) calculations. The rhombohedral angle, on the other hand, is in excellent agreement with experiment. The three bond lengths which differ the most between B_{12}(CCC) and $B_{11}C$(CBC) are *wC*, *ab*, and *CB*. In each case the $B_{11}C$(CBC) result is in far better agreement with experiment.

The various contributions to the cohesive energy of B_{12}(CCC) and $B_{11}C$(CBC) are listed in Table IV. The first term is the sum of the one-electron eigenvalues. Subtracting off the valence electron potential contribution to these eigenvalues (terms 2 and 3) makes the calculation variational.[19,20] Terms 4 and 5 add the valence electron self-Coulomb and exchange-correlation energies and term 6, the Ewald-Madelung energy, is the energy of C^{4+} and B^{3+} point ions at their equilibrium positions with a constant background of compensating electronic charge density. The total energy is converged to six decimal places although by comparing $\int V^{\text{in}}_{\text{Coul}}\rho_{\text{out}}$ with $2E_{\text{Coul}}$ one can see that the individual contributions are not. The atomic energy which is subtracted from $-E_{\text{Total}}$ to obtain the cohesive energy is $E_{\text{Atomic}}=\frac{1}{5}(4E_B+E_C)$ where these boron and carbon atomic total energies were calculated to be $E_B=-5.170\,92$ Ry, $E_C=-10.749\,80$ Ry. By adding the heat of formation[2(b)] of B_4C to $\frac{4}{5}$ the cohesive energy[21] of B and $\frac{1}{5}$ that of C an experimental value of 6.27 eV/atom for the cohesive energy of $B_{12}C_3$ is obtained. It is not unusual for LDA calculations to result in a large overestimate of the cohesive energy of refractory com-

TABLE II. List of all bond lengths in bohrs calculated for $B_{11}C$(CBC). Bonds which become equivalent in B_{12}(CCC) are grouped together.

$dk=dv=3.3141$, $wg=wh=3.3310$, $vg=kh=3.2868$; $ak=bv=3.3630$,
$cw=3.3030$, $xh=yg=3.3489$, $zd=3.4097$; $ad=bd=3.3704$, $cg=ch=3.3288$,
$bg=ah=3.4103$, $zk=zv=3.4193$, $yw=xw=3.3632$, $xk=yv=3.4114$; $ab=3.4169$,
$ca=cb=3.3676$, $xy=3.4230$, $zx=zy=3.4434$; $cz=3.1674$, $xb=ya=3.2592$; $wC=3.0025$,
$Ck=Cv=3.0340$, $Kd=3.0269$, $Kg=Kh=3.0309$; $CB=2.7036$, $KB=2.7441$

TABLE III. Rhombohedral lattice constant and angle, unit-cell volume and bond lengths for B_{12}(CCC) and the rhombohedral averages of the same quantities for $B_{11}C$(CBC) compared with experiment (Ref. 4). 6*dk* refers to a group of six equivalent bonds of which *dk* is a member.

	B_{12}(CCC)	$B_{11}C$(CBC)	Expt.
a (bohr)	9.7933	9.7180	9.7606
α	65.607°	65.758°	65.71°
Ω (bohr^3)	745.036	729.848	738.94
6*dk* (bohr)	3.3103	3.3106	3.330
6*ak* (bohr)	3.3531	3.3561	3.377
12*ad* (bohr)	3.3830	3.3839	3.405
6*ab* (bohr)	3.4715	3.4103	3.417
3*cz* (bohr)	3.2489	3.2286	3.241
6*wC* (bohr)	3.1032	3.0235	3.035
2*CB* (bohr)	2.5537	2.7239	2.7082

pounds (e.g., $MoSi_2$).[22] Nevertheless, the difference between cohesive energies of two atomic configurations of the same compound is expected to be quite accurate. This is because the LDA underestimates the total energy of both the atom and the solid but has a much larger error for the atom;[23] the atomic energy cancels out of the difference between two cohesive energies. Although the two cohesive energies in Table IV do not differ by a large amount, when multiplied by 15 to get the difference per unit cell, we find it requires 1.282 eV to interchange the chain boron and the icosahedral carbon atoms. Thus, consistent with what we concluded by comparing equilibrium bond lengths with x-ray data, we assert from total energy calculations that the correct atomic configuration of $B_{12}C_3$ is $B_{11}C$(CBC).

In Fig. 2 the energy bands of $B_{11}C$(CBC) are plotted in the reflection plane. We use Slater's[24] notation for the rhombohedral BZ symmetry points in spite of the fact that our BZ does not have that symmetry. The *Z* and *A* points are in the centers of regular and distorted hexagonal faces and *B* in the center of a rectangular face of the BZ. *U*, which was not denoted by Slater since it has no extra symmetry, is at the intersection of the rectangular and distorted hexagonal faces. Bands in the directions

TABLE IV. Contributions to cohesive energies of B_{12}(CCC) and $B_{11}C$(CBC) calculated in their equilibrium configurations (in Ry/atom).

	B_{12}(CCC)	$B_{11}C$(CBC)
$\Sigma\epsilon_{nk}$	0.428 91	0.520 43
$-\int V^{\text{in}}_{\text{Coul}}\rho_{\text{out}}$	−1.897 02	−1.832 44
$-\int V^{\text{in}}_{\text{xc}}\rho_{\text{out}}$	3.138 00	3.150 80
E_{Coul}	0.948 60	0.916 88
E_{xc}	−2.417 72	−2.428 04
E_{Ewald}	−7.014 73	−7.147 87
E_{Total}	−6.813 96	−6.820 24
E_{Atom}	−6.286 70	−6.286 70
E_{coh} (eV/atom)	7.173	7.259

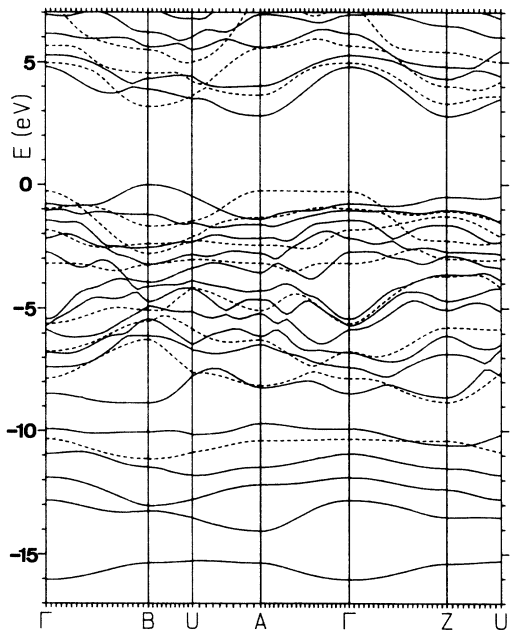

FIG. 2. Energy bands plotted in the reflection plane of $B_{11}C$(CBC). The dashed bands are odd under reflection and the solid ones even.

opposite to *BU*, *UA*, and *ZU* are identical to them via a reciprocal lattice vector translation and time reversal. Thus Fig. 2 shows the bands in three directions away from Γ as well as along the entire intersection of the reflection plane with the BZ surface. The dashed bands are odd under reflection and the solid ones even. The tops of the valence bands are at *B* and the bottoms of the conduction bands at *A* although *Z* is only 0.0225 eV higher. The indirect gap is 2.781 eV and the direct gaps at *A*, *B*, and *Z* are 3.050, 3.170, and 3.272 eV, respectively. These gaps may be compared with the 3.8-eV gap Bullett[9] obtained in the density of states of B_{12}(CCC) with a much less sophisticated calculation. We know of no other calculations nor of any optical or photoemission data with which to compare our results. We remind the reader that the LDA results in gaps that are too small by 0.7 eV or more in the diamond and zinc-blende semiconductors and similar discrepancies here would not be surprising.

Figure 3 is a plot of contours of constant pseudocharge density in the reflection plane (in units of millielectrons per cubic bohr, me/a_0^3). Pseudocharge is depleted in the atomic cores and the small closed 40 (120) contours are the boron (carbon) cores. Starting from the θ point (see Fig. 1 for the notation) and going along the $\theta\varphi$ edge we pass though[25] boron atom *z* to carbon *c* which bonds to *w* below it and it to the *CBK* chain. *K* in turn bonds to *d* and it to *z* to *c* in the $\pi\rho$ edge. Note that the carbon charge-density peaks at 280 along the intericosahedral *cz* bond, at 240 along the intraicosahedral *cw* bond, at 280 along the icosahedron-chain *wC* bond and at 320 along the intrachain *CB* and *BK* bonds, in inverse order of bond length. Note also that the minimal contour is 8 me/a_0^3

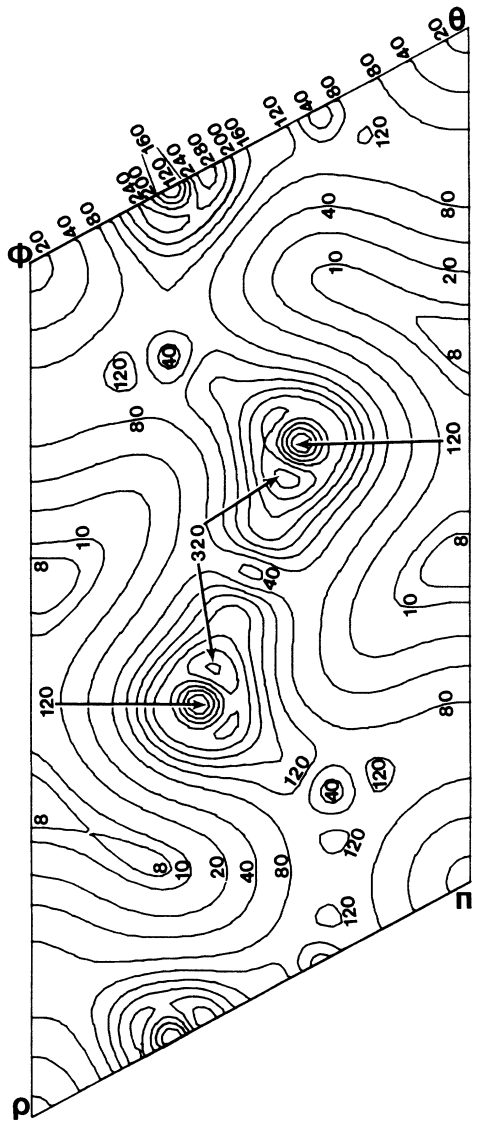

FIG. 3. Contours of constant charge density in the $\theta\varphi\rho\pi$ reflection plane of B_{11}(CBC). The contours (in millielectrons per cubic bohr) go in steps of 2 up to 10, then 20 and 40 and in steps of 40 up to 320.

which is equivalent to $r_s = 3.1$, i.e., the charge density in the interstitial voids of $B_{12}C_3$ is larger than the average charge density in lithium metal, $r_s = 3.25$. Figure 4 is a plot of constant charge-density contours in all 12 independent faces of the icosahedron. The remaining eight faces are reflection images of those plotted (in either the *cd* or *wz* lines). We see that except around the carbon (where it is larger) and in the boron cores (where it is smaller) the charge is fairly evenly spread out over the icosahedral surface with an $r_s \approx 1.25$. It appears from both Figs. 3 and 4 that the ratio of the charge around the carbon atoms to that around the boron is much larger than the 4:3 ratio of their valences. To check this we analytically integrated the plane-wave expansion of the charge density in spheres about each atom. The results for spheres whose radii are half the *CB* and *Ck* bond lengths (in Table II) are listed in Table V. The smaller spheres fill 21.27% of the unit-cell volume and contain 40.04% of the charge. We also calculated the charge within a sphere of 4.5767 bohr radius surrounding an icosahedron.[26] This sphere contains 55.02% of the unit-cell volume and 28.112*e* or 58.57% of the charge.

Thus a picture of the $B_{12}C_3$ bonding emerges. The intraicosahedral bonding is essentially that of a very dense two-dimensional metal. The icosahedral carbon contributes an extra electron but the carbon electrons could be so tightly bound that those four electrons actually contribute less to the bonding than the three electrons on each boron atom. On the other hand, the B_{12} icosahedron is two electrons short of the full complement of bonding orbitals,[8] and although the carbon charge is not spread over the whole icosahedron, its extra electron might still contribute significantly to the bonding. When our $B_{13}C_2$ calculations are completed, we will have the answer. Each icosahedron bonds to four other icosahedra with boron-boron bonds and to two with boron-carbon bonds. If one considers both the maximum amplitude and total charge in a bond as a measure of its strength, the so-called three-center[3] intraicosahedral boron-boron bonds are much stronger than the intericosahedral bonds in spite of the fact that they are longer, whereas for the boron-carbon bonds the case is not so obvious. What does appear clear, however, is that the intericosahedral *cz* and icosahedral-chain *wC* and *Kd* bonds are of approximately equal strength.

To gain further insight into the nature of the bonding we have examined charge-density–contour plots of individual eigenfunctions (all at the *B* point in the BZ). The lowest band is a carbon *c* wave function which has an amplitude of 15 me/a_0^3 at the nucleus, peaks at 27 me/a_0^3 slightly *inside* the icosahedron, falls off very rapidly along the *cz* bond, and is moderately spread out over the five faces of the icosahedron that *c* touches. Its largest contour in a face is 21 me/a_0^3. The next band is a carbon *C* wave function of 23 me/a_0^3 at the nucleus. It falls to 20 me/a_0^3 at 30% of the way along its three bonds to icosahedral borons and then falls much more rapidly. Its peak of 39 me/a_0^3 occurs right at the peak of the total

TABLE V. Integrated charge about atoms in spheres with radii $R_1 = 1.3518$ bohr and $R_2 = 1.5168$ bohr (half the *CB* and *Ck* bond lengths, respectively).

Atom	$Q(R_1)$	$Q(R_2)$
K	2.159	2.736
B	1.075	1.466
C	2.176	2.758
x,y	1.069	1.454
a,b	1.055	1.437
c	1.971	2.429
z	1.040	1.416
d	1.098	1.500
w	1.091	1.492
g,h	1.085	1.483
k,v	1.096	1.497

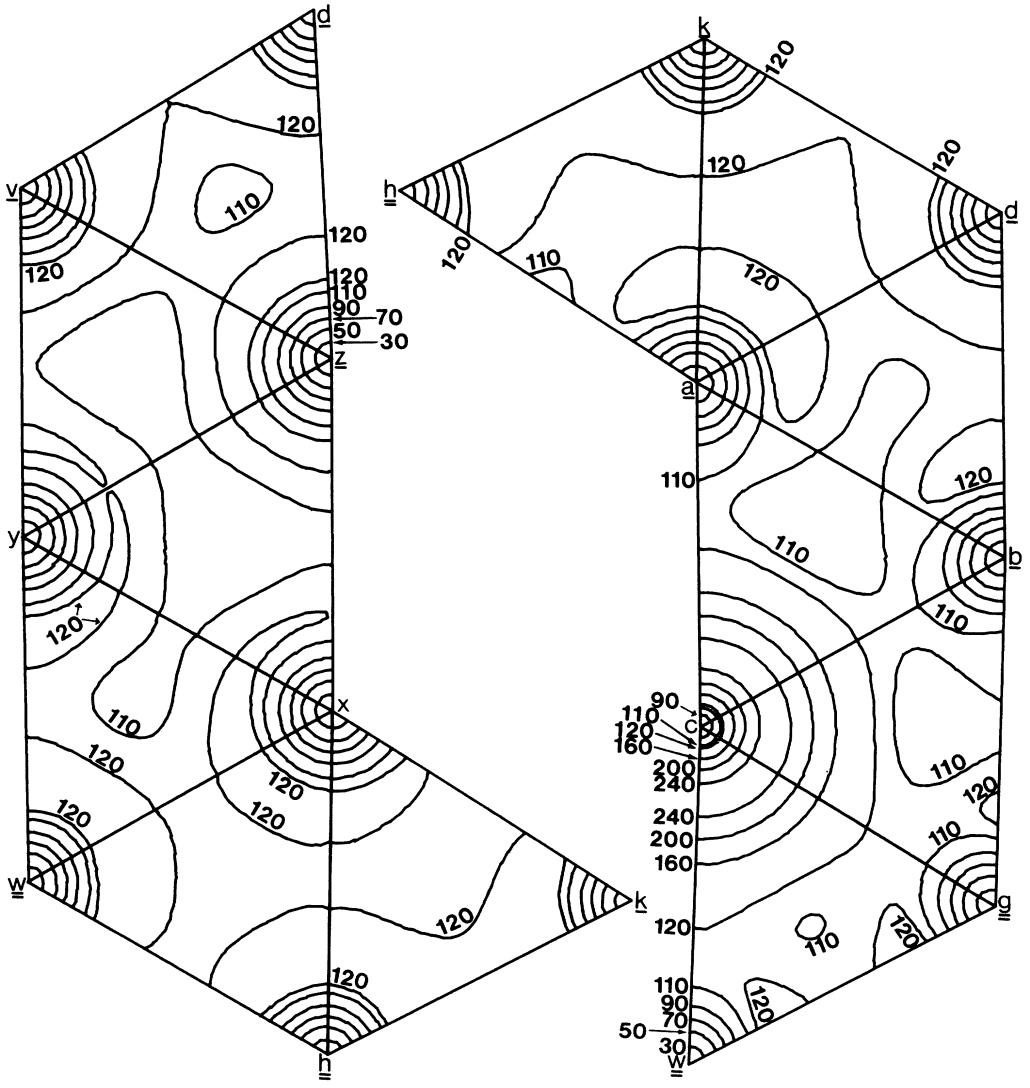

FIG. 4. Contours of constant charge density in the surface of the $B_{11}C(CBC)$ icosahedron. The atoms are labeled as in Fig. 1 and the number of lines under the label is the number of carbon neighbors the atom has. The contours plotted are 30, 50, 70, 90, 110, and 120 millielectrons per cubic bohr.

charge density in the *CB* bond but it falls very rapidly beyond this peak. The third band is essentially identical to the second but with carbon *K* instead of *C*. The fourth band is the lowest icosahedral state. It peaks *very* sharply at 18 me/a_0^3 just above the *abc* face and close to *c*. Nevertheless this eigenfunction has considerably larger charges in the triangles on the left side of Fig. 4 than on the right. There is an 11 me/a_0^3 contour around the center of the *xy* bond and the two triangles sharing that bond have about 60% of their area within the 9 me/a_0^3 contour whereas the *abc* triangle has about $\frac{1}{3}$ of its area within that contour and has no higher contour. Band 5 is the first one odd under reflection. Along the four icosahedron-chain bonds not in the reflection plane it has a small charge density which grows from zero at the *C* or *K* chain atoms to about 3 me/a_0^3 and then drops slowly to about 1 me/a_0^3 before increasing to about 1.5 me/a_0^3 on the icosahedral boron atom. A large fraction of this eigenfunction lies within the icosahedra. Going perpendicularly away from the reflection plane at the center of an icosahedron, the charge peaks at just above 9 me/a_0^3 about $\frac{2}{3}$ of the way to the surface of the icosahedron. Some of the icosahedral faces contain small closed 6 me/a_0^3 contours but most of the faces have either 3 or 1 me/a_0^3 contours as their largest. Band 6 has charge peaking at 21 me/a_0^3 near carbon *c*, 12me/a_0^3 near boron *d*, and 15 me/a_0^3 near *C* and *K*. Although this charge density peaks sharply near several bonding atoms, it appears to be antibonding. The *K* and *d* peaks appear to repel and the charge density drops below 0.5 me/a_0^3 between them. The *c* peak is displaced towards *w* where $\rho < 0.5$ me/a_0^3 and the *C* peak toward *B* where $\rho = 1$ me/a_0^3. The out of plane *Kg* and *Kh* bonds peak at 10 me/a_0^3 near *K* and fall to 0.5 at *g* or *h*. The *Ck* and *Cv*

bond charge is much smaller. Thus of the six lowest bands, two appear to contribute to intraicosahedral bonding and the other four appear to be strongly bound because they contain mainly carbon s orbitals.

At the top of the valence bands the 24th level looks like σp orbitals on C, B, and K overlapping in phase. The charge density peaks at 12 me/a_0^3 on C and K away from B and at 21 me/a_0^3 toward B. It peaks above 18 me/a_0^3 on both sides of B and never falls below 18 in the midbond regions. In addition this wave function peaks with $\rho > 12$ me/a_0^3 about $\frac{1}{3}$ and $\frac{2}{3}$ of the way along the intraicosahedral ab bond and stays above 9 me/a_0^3 over the middle $\frac{3}{4}$ of the bond. This is the only occupied eigenfunction that appears to contain a large component of B orbitals, the B $2s$ orbitals being hybridized into many diffuse functions. Band 23 consists mainly of carbon c and boron z intericosahedral bonding σp orbitals. Near c the bond charge peaks at 54 me/a_0^3 with a large midbond region with $\rho > 24$ me/a_0^3. On the other side of c and k the charge peaks at 39 and 15 me/a_0^3, respectively. This eigenstate also contains some Ck, Cv, Kg, and Kh chain-icosahedron bonding. From about 1.5 me/a_0^3 at K, ρ increases to 10 me/a_0^3 at 25% of the way to g or h. It falls to 5 me/a_0^3 at 75% of the way and then to zero at g or h. The Ck and Cv charge is about 15% smaller except near k and v. In the reflection plane between the Kg and Kh (or Ck and Cv) charge-density maxima, the charge peaks at 21 me/a_0^3 but only at 9 me/a_0^3 in the opposite direction from the carbon atoms so that in the plane it looks like a bonding orbital pointing toward nothing. Bands 21 and 22 are both mainly odd chain-icosahedral bonding orbitals. We plot them along the bonding directions in Fig. 5. Although ρ is very small at the icosahedral bo-

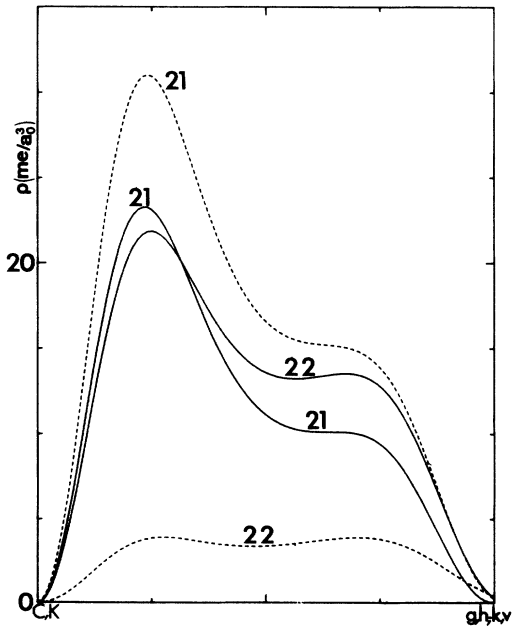

FIG. 5. Plot of the charge density of the 21st and 22nd bands at B in the BZ plotted along the Kg or Kh (dashed curve) and Ck or Cv (solid curves) bonds.

rons g, h, k, and v, in band 22 it rapidly increases to also form intraicosahedral gd, hd, kd, and vd bonds which peak above 15 me/a_0^3. In band 21, the charge peaks inside a 9 me/a_0^3 contour in the yzv (and xzk) triangle and remains above 9 me/a_0^3 over about 60% of that face. Band 20 is a carbon c boron z intericosahedral π bond (it could also contain boron-boron intericosahedral π bonds but those charge lobes are in directions in which we do not look). Band 19 is odd and peaks at 33 me/a_0^3 along bx and ay intericosahedral bonds. Thus all the states near the top of the valence bands show bonding character. Above the gap band 25 and 26 are diffuse but show some bonding character whereas band 27 shows antibonding π character. It is very localized on boron B with a maximum $\rho = 77$ me/a_0^3. The carbons K and C have maxima of only 15 me/a_0^3.

In conclusion, we have confirmed that the ground-state configuration of B_4C is $B_{11}C(CBC)$ rather than $B_{12}(CCC)$, both from the total energy calculations and from a comparison of calculated internuclear separations with x-ray data. In addition, we have discussed the nature of the bonding, both from a consideration of individual eigenstates, as well as total charge density which gave a picture of metallic icosahedral surfaces covalently bonded to each other and to the CBK chain.

ACKNOWLEDGMENTS

This work was supported by the Robert A. Welch Foundation (Houston, Texas), the University of Texas Center for High Performance Computing, and the National Science Foundation under Grant No. DMR-8718048.

APPENDIX A

Our computational method is a variation on a theme by Teter, Payne, and Allan.[27] Our method is doubly iterative in that we use an iterative method to improve each approximate eigenfunction at each $\mathbf{k}$ sampled in the BZ (we call these subiterations) and then diagonalize a matrix of the improved approximate eigenfunctions to obtain starting eigenfunctions for the next iteration which begins after the crystal potential has been updated. Define $\psi_{n\mathbf{k}}^{(0)}(j,i)$ to be the approximate eigenfunction for the nth band at $\mathbf{k}$ in the ith subiteration of the jth iteration. Then since

$$\delta E_{n\mathbf{k}}/\delta\psi_{n\mathbf{k}}^{(0)*} = (H - E_{n\mathbf{k}})|\psi_{n\mathbf{k}}^{(0)}\rangle / \langle\psi_{n\mathbf{k}}^{(0)}|\psi_{n\mathbf{k}}^{(0)}\rangle$$

where

$$E_{n\mathbf{k}} = \langle\psi_{n\mathbf{k}}^{(0)}|H|\psi_{n\mathbf{k}}^{(0)}\rangle / \langle\psi_{n\mathbf{k}}^{(0)}|\psi_{n\mathbf{k}}^{(0)}\rangle ,$$

$$|\psi_{n\mathbf{k}}^{(1)}\rangle = (H - E_{nk})|\psi_{n\mathbf{k}}^{(0)}\rangle \quad \text{(A1)}$$

lies in the direction of steepest descents in the Hilbert space of the basis functions (plane waves in our case) from which $\psi_{n\mathbf{k}}$ is constructed. If the direction of steepest descents changed only slowly in the Hilbert space, one could diagonalize the 2×2 matrix of H between $\psi_{n\mathbf{k}}^{(1)}(j,i)$ and $\psi_{n\mathbf{k}}^{(0)}(j,i)$ to obtain a much improved $\psi_{n\mathbf{k}}^{(0)}(j,i+1)$. One can see, however, that the kinetic ener-

gy operator in H will cause the plane waves with largest $\mathbf{k}+\mathbf{G}$ to have the largest coefficients in $\psi_{n\mathbf{k}}^{(1)}$ (where $\mathbf{G}$ is a reciprocal lattice vector). Since the converged valence-band wave functions have only a small component of high kinetic energy plane waves, it is obvious that only a small amount of $\psi_{n\mathbf{k}}^{(1)}(j,i)$ will admix with $\psi_{n\mathbf{k}}^{(0)}(j,i)$ and that $\psi_{n\mathbf{k}}^{(0)}(j,i+1)$ will be only a small improvement over $\psi_{nk}^{(0)}(j,i)$. There are two improvements that can be made to $\psi_{n\mathbf{k}}^{(1)}(j,i)$. The first, called preconditioning,[27] involves multiplying the coefficient of each plane wave in $\psi_{n\mathbf{k}}^{(1)}$ by a factor which is unity if $x=\frac{1}{2}(\mathbf{k}+\mathbf{G})^2-T<0$, where T is the average kinetic energy of $\psi_{n\mathbf{k}}^{(0)}$, and which goes from unity at $x=0$ to something proportional to $1/x$ at large x. (We used the factor used in Ref. 27.) Thus, calling the preconditioning operator P, and O the operator which orthogonalizes $\psi_{n\mathbf{k}}^{(1)}(j,i)$ to all the $\psi_{m\mathbf{k}}^{(0)}(j,i_{\max})$ with $m<n$, to $\psi_{n\mathbf{k}}^{(0)}(j,i)$ and to all the $\psi_{m\mathbf{k}}^{(0)}(j,0)$ with $m>n$ we have

$$|\psi_{n\mathbf{k}}^{(2)}(j,i)\rangle = OP(H-E)|\psi_{n\mathbf{k}}^{(0)}(j,i)\rangle \ . \tag{A2}$$

The conjugate gradient algorithm changes the vector in function space from one which points in the direction of steepest descents to one which points more nearly to the minimum in $E_{n\mathbf{k}}$. [If one is close enough to the minimum that $E_{n\mathbf{k}}$ is a quadratic function of the coefficients of the basis functions, the vector points exactly to the minimum in the subspace spanned by $\psi_{n\mathbf{k}}^{2}(j,i)$ and $\psi_{n\mathbf{k}}^{(3)}(j,i-1)$.] Thus

$$|\psi_{n\mathbf{k}}^{(3)}(j,i)\rangle = |\psi_{n\mathbf{k}}^{(2)}(j,i)\rangle + \gamma_i |\psi_{n\mathbf{k}}^{(3)}(j,i-1)\rangle \tag{A3}$$

with

$$\gamma_i = \frac{\langle \psi_{n\mathbf{k}}^{(2)}(j,i)|\psi_{n\mathbf{k}}^{(2)}(j,i)\rangle}{\langle \psi_{n\mathbf{k}}^{(2)}(j,i-1)|\psi_{n\mathbf{k}}^{(2)}(j,i-1)\rangle} \tag{A4}$$

for $i>1$ and $\gamma_1=0$. Since $\psi_{n\mathbf{k}}^{(3)}(j,i-1)$ was constructed to be orthogonal to all the $\psi_{m\mathbf{k}}^{(0)}$ and only $\psi_{n\mathbf{k}}^{(0)}$ has changed from the previous subiteration, all that remains to be done is to orthogonalize $\psi_{n\mathbf{k}}^{(3)}(j,i)$ to $\psi_{n\mathbf{k}}^{(0)}(j,i)$ and to normalize it. Thus

$$\begin{aligned}|\psi_{n\mathbf{k}}^{(5)}(j,i)\rangle &= N|\psi_{n\mathbf{k}}^{(4)}(j,i)\rangle \\ &= N[|\psi_{n\mathbf{k}}^{(3)}(j,i)\rangle - |\psi_{n\mathbf{k}}^{(0)}(j,i)\rangle \\ &\quad \times \langle \psi_{n\mathbf{k}}^{(0)}(j,i)|\psi_{n\mathbf{k}}^{(3)}(j,i)\rangle]\end{aligned} \tag{A5}$$

where $N=[\langle \psi_{n\mathbf{k}}^{(4)}(j,i)|\psi_{n\mathbf{k}}^{(4)}(j,i)\rangle]^{-1/2}$. The 2×2 Hamiltonian matrix between $\psi_{n\mathbf{k}}^{(0)}(j,i)$ and $\psi_{n\mathbf{k}}^{(5)}(j,i)$ is then diagonalized to obtain $\psi_{n\mathbf{k}}^{(0)}(j,i+1)$. These subiterations are performed $i_{\max}$ times to obtain $\psi_{n\mathbf{k}}^{(0)}(j,i_{\max})$ for each band in succession at a particular $\mathbf{k}$ up to $n=n_{\max}$. We took $n_{\max}=25$ to include the lowest conduction band. We then diagonalize the 25×25 Hamiltonian matrix between the $\psi_{n\mathbf{k}}^{(0)}(j,i_{\max})$ to obtain the $\psi_{n\mathbf{k}}^{(0)}(j+1,0)$. That preconditioning[28] and the conjugate gradient[29] work individually to improve the convergence can be demonstrated mathematically. That they work simultaneously has also been mathematically demonstrated[30] (although in a context slightly different than ours) and our calculation demonstrates their simultaneous efficacy empirically.

After obtaining the $\psi_{n\mathbf{k}}^{(0)}(j+1,0)$ for all $\mathbf{k}$ sampled in the BZ, the charge density, and the valence electron potential (Coulomb and exchange correlation) which is the output of the jth iteration, V_j^{out}, is calculated and a weighted average of the discrepancy between input and output Fourier transforms of V_j is added to V_j^{in} to obtain V_{j+1}^{in}:

$$V_{j+1}^{\text{in}}(\mathbf{G}) = V_j^{\text{in}}(\mathbf{G}) + AG^2 \frac{V_j^{\text{out}}(\mathbf{G})-V_j^{\text{in}}(\mathbf{G})}{G^2+B(2\pi/a)^2} \ . \tag{A6}$$

We found $A=0.5$ and $B=1.92$ with $a=9.718$ bohr (see Table III) to give satisfactory results. The deweighting of the long wavelength (small $\mathbf{G}$) corrections to the potential prevents charge sloshing. Teter *et al.*[27] prevented charge sloshing by updating the potential after the calculation of each new eigenfunction. This is not only time consuming, we have seen[31] that it can actually worsen the potential because the charge density of a single electron is vastly different from that of the average of all electrons. There are two steps in our procedure that may seem wasteful of computer time but they are not. The construction of the 25×25 matrix uses very little time because the $H\psi_{n\mathbf{k}}^{(0)}(j,i_{\max})$ have essentially been calculated previously so that the matrix elements involve only a single dot product. A small improvement in the total energy of the jth iteration is obtained because of the inclusion of the one conduction-band state. The real gain comes from the improvement of the $\psi_{n\mathbf{k}}^{(0)}(j+1,0)$ over the $\psi_{n\mathbf{k}}^{(0)}(j,i_{\max})$ which results in a large improvement in the total energy of the $(j+1)$st iteration. It appears time would be saved if the orthogonalization operator in Eq. (A2) did not orthogonalize $\psi_{n\mathbf{k}}^{(1)}(j,i)$ to the $\psi_{m\mathbf{k}}^{(0)}(j,0)$ with $m>n$ but instead orthogonalized the $\psi_{n\mathbf{k}}^{(0)}(j,0)$ to the $\psi_{m\mathbf{k}}^{(0)}(j,i_{\max})$ with $m<n$ because the former operation is performed once per subiteration and the latter once per iteration. However, we find that the orthogonalization of the $\psi_{n\mathbf{k}}^{(0)}(j,0)$ so increases their energy that iterations occur in which the total energy increases and it is impossible to converge to the true total energy. In fact, the better one calculates the lower bands (e.g., by including preconditioning and the conjugate gradient or by increasing $i_{\max}$) the worse the effect is. We noticed this effect previously[31] but wrongly attributed it to a numerical instability. Finally, we come to the values of $i_{\max}$ and $j_{\max}$. We iterate until the total energy is converged to about 10^{-6} Ry/atom which requires $j_{\max}\sim8$. In every iteration except the first we find that the first subiteration gives a large decrease in $E_{n\mathbf{k}}$ as does the second (because this is the first subiteration that contains the conjugate gradient) and subsequent iterations give much smaller improvements. These small improvements are of little value since the eigenfunction toward which one is converging will be changed at the end of the iteration when the potential is updated. Therefore $i_{\max}=2$ for $j\neq1$. For $j=1$ the potential, which is constructed from a superposition of atomic charge densities, is a fair approximation to the converged potential, whereas the $\psi_{n\mathbf{k}}^{(0)}(1,0)$ have coefficients whose real and imaginary parts are completely random except for a multiplicative factor to deweight the larger $(\mathbf{k}+\mathbf{G})$. Thus in order to bring the quality of

the wave functions up to the quality of the potential we took $i_{\max}=5$ for $j=1$. Also, because the $\psi^{(0)}_{n\mathbf{k}}(1,0)$ are not orthogonal to one another we did not orthogonalize $\psi^{(1)}_{n\mathbf{k}}(1,i)$ to the $\psi^{(0)}_{m\mathbf{k}}(1,0)$ with $m>n$ but rather orthogonalized the $\psi^{(0)}_{n\mathbf{k}}(1,0)$ to the $\psi^{(0)}_{m\mathbf{k}}(1,i_{\max})$ with $m<n$. With $i_{\max}=2$ it took about 205 sec of Cray XMP CPU time per complete $B_{11}C$(CBC) iteration and about 105 sec for B_{12}(CCC), the difference arising from the fewer independent $\mathbf{k}$'s sampled in the BZ in the higher symmetry case. For $i_{\max}=5$, the time required was somewhat less than twice as much.

APPENDIX B

After each calculation for the total energy was converged, we moved each atom within the unit cell an amount proportional to the force acting on it and recalculated the energy and the forces. This was done about three times until the forces were relaxed and then we strained the primitive lattice vectors proportionally to the stress tensor, usually twice. The entire process was repeated four times until the energy, as a function of lattice vectors and atomic positions, was converged to within 3×10^{-5} Ry/atom. The force and stress formulas are given in Refs. 32 and 33 except that these authors used a semilocal pseudopotential of the form

$$V_{Ps}(\mathbf{r})=V_L(r)+\sum_{lm}|Y_{lm}(\theta,\varphi)\rangle V_l(r)\langle Y_{lm}(\theta,\varphi)|$$

where Y_{lm} is a spherical harmonic and we use a nonlocal

$$V_{Ps}(\mathbf{r})=V_L(r)+\sum_{lm}|Y_{lm}(\theta,\varphi)v_l(r)\rangle\langle v_l(r)Y_{lm}(\theta,\varphi)|\ .$$

Therefore we list below the pseudopotential contribution to the force and stress tensor:

$$\mathbf{F}_\tau=\Omega\sum_{\mathbf{G}}i\mathbf{G}e^{-i\mathbf{G}\cdot\tau}V_{L\tau}(\mathbf{G})\rho^*(\mathbf{G})$$
$$-i\sum_{n,\mathbf{k};l,m}\left[\left[\sum_{\mathbf{G}}C^*_{n,\mathbf{k}+\mathbf{G}}v_{\tau l}(\mathbf{k}+\mathbf{G})Y_{lm}(\mathbf{k}+\mathbf{G})e^{-i\mathbf{G}\cdot\tau}\right]\left[\sum_{\mathbf{G}}C_{n,\mathbf{k}+\mathbf{G}}v_{\tau l}(\mathbf{k}+\mathbf{G})Y^*_{lm}(\mathbf{k}+\mathbf{G})e^{i\mathbf{G}\cdot\tau}(\mathbf{k}+\mathbf{G})\right]+\text{c.c.}\right] \quad \text{(B1)}$$

where τ is the vector from the lattice site to the τth atom in the unit cell of volume Ω and the $C_{n,\mathbf{k}+\mathbf{G}}$ are the coefficients of the plane waves in $\psi_{n,\mathbf{k}}$. The sum on n is over occupied bands and the $\mathbf{k}$ sum means average over the BZ. We write

$$\sigma_{\alpha\beta}=-\Omega\sum_{\mathbf{G},\tau}e^{-i\mathbf{G}\cdot\tau}[\delta_{\alpha\beta}V_{L\tau}(G)-(G_\alpha G_\beta/G)\tilde{V}_{L\tau}(G)]$$
$$+\sum_{n,\mathbf{k},\tau}\sum_{l,m}\left[\left[\sum_{\mathbf{G}}C^*_{n,\mathbf{k}+\mathbf{G}}v_{\tau l}Y_{lm}(\mathbf{k}+\mathbf{G})e^{-i\mathbf{G}\cdot\tau}\right]\right.$$
$$\left.\times\left[\sum_{\mathbf{G}}C_{n,\mathbf{k}+\mathbf{G}}e^{i\mathbf{G}\cdot\tau}[-\tfrac{1}{2}\delta_{\alpha\beta}v_{\tau l}(\mathbf{k}+\mathbf{G})+\bar{v}_{\tau l}(\mathbf{k}+\mathbf{G})Y^*_{lm}(\mathbf{k}+\mathbf{G})(k_\alpha+G_\alpha)(k_\beta+G_\beta)/|\mathbf{k}+\mathbf{G}|]\right]+\text{c.c.}\right] \quad \text{(B2)}$$

where

$$V_{L\tau}(G)=(4\pi/\Omega)\int_0^\infty r^2j_0(Gr)[V_{L\tau}(r)+\delta_{G,0}Z_\tau/r]dr\ , \quad \text{(B3)}$$

$$\tilde{V}_{L\tau}(G)=(4\pi/\Omega)\int_0^\infty r^3j_1(Gr)V_{L\tau}(r)dr\ , \quad \text{(B4)}$$

$$v_{\tau l}(\mathbf{k}+\mathbf{G})=(4\pi/\Omega^{1/2})\int_0^\infty r^{l+2}j_l(|\mathbf{k}+\mathbf{G}|r)v_{\tau l}(r)dr\ , \quad \text{(B5)}$$

$$\bar{v}_{\tau l}(\mathbf{k}+\mathbf{G})=[4\pi/(2l+1)\Omega^{1/2}]\times\int_0^\infty[(l+1)j_{l+1}(|\mathbf{k}+\mathbf{G}|r)-lj_{l-1}(|\mathbf{k}+\mathbf{G}|r)]v_{\tau l}(r)r^{l+3}dr\ , \quad \text{(B6)}$$

and the j_l are spherical Bessel functions.

APPENDIX C

We here describe how we chose our 32-point sample in the BZ. Using lattice vectors $\mathbf{R}_1=\theta\varphi$, $\mathbf{R}_2=\theta\varphi$, and $\mathbf{R}_3=\theta\omega$ given in Table I, the reciprocal lattice vectors $\mathbf{G}_i=2\pi(\mathbf{R}_j\times\mathbf{R}_k)/(\mathbf{R}_i\cdot\mathbf{R}_j\times\mathbf{R}_k)$ of $B_{11}C$(CBC) are found to be (in inverse bohr)

$$\mathbf{G}_1=2\pi(-0.111\,14,0,-0.044\,02)\ , \quad \text{(C1)}$$

$$\mathbf{G}_2=2\pi(0.053\,66,-0.094\,43,-0.044\,02)\ , \quad \text{(C2)}$$

$$\mathbf{G}_3=2\pi(0.053\,66,0.094\,43,-0.044\,02)\ . \quad \text{(C3)}$$

Now if there were no distortions and the angles between $\mathbf{R}_1$, $\mathbf{R}_2$, and $\mathbf{R}_3$ were all 60°, the matrix $\mathcal{R}$ would rotate our Cartesian coordinates into the usual cubic coordinates of the fcc lattice, where

$$\mathcal{R}=\begin{bmatrix}1/\sqrt{6} & -1/\sqrt{2} & 1/\sqrt{3}\\ 1/\sqrt{6} & 1/\sqrt{2} & 1/\sqrt{3}\\ -2/\sqrt{6} & 0 & 1/\sqrt{3}\end{bmatrix}\ . \quad \text{(C4)}$$

We find

$$\mathcal{R}\mathbf{G}_1=2\pi(-0.070\,79,-0.070\,79,0.065\,33)\ ,$$

$$\mathcal{R}\mathbf{G}_2=2\pi(0.063\,26,-0.070\,28,-0.069\,23)\ ,$$

$$\mathcal{R}\mathbf{G}_3=2\pi(-0.070\,28,0.063\,26,-0.069\,23)\ ,$$

so that $\mathbf{G}_1$, $\mathbf{G}_2$, and $\mathbf{G}_3$ are distorted fcc (1,1,1) reciprocal lattice vectors. Therefore we sample the BZ at the eight points corresponding to fcc $(\frac{1}{4},\frac{1}{4},\frac{1}{4})$ points and the 24 corresponding to fcc $(\frac{3}{4},\frac{1}{4},\frac{1}{4})$ points: $\mathbf{k}_{1,2}=\pm\frac{1}{4}\mathbf{G}_1$, $\mathbf{k}_{3,4}=\pm\frac{1}{4}\mathbf{G}_2$, $\mathbf{k}_{5,6}=\pm\mathbf{G}_3$, $\mathbf{k}_{7,8}=\pm\frac{1}{4}(\mathbf{G}_1+\mathbf{G}_2+\mathbf{G}_3)$, $\mathbf{k}_{9-14}=\pm\frac{1}{4}(2\mathbf{G}_1+\mathbf{G}_2)$ and cyclic permutations (CP), $\mathbf{k}_{15-20}=\pm\frac{1}{4}(2\mathbf{G}_2+\mathbf{G}_1)$ and CP, $\mathbf{k}_{21-26}=\pm(\mathbf{G}_3-\mathbf{G}_1-\mathbf{G}_2)$ and CP, $\mathbf{k}_{27-32}=\pm\frac{1}{4}(2\mathbf{G}_1+2\mathbf{G}_2+\mathbf{G}_3)$ and CP. Time reversal and the reflection plane which interchanges $\mathbf{G}_1$ and $\mathbf{G}_2$ reduce the eight points to three and the 24 points to seven independent ones. For B_{12}(CCC) these further reduce to two and three. At each $\mathbf{k}$ point we used all plane waves such that $(\mathbf{k}+\mathbf{G})^2<43.346$ Ry for B_{12}(CCC) and 43.946 Ry for B_{11}C(CBC) where the maximum kinetic energy is scaled by $\Omega^{-2/3}$. It is not obvious whether two calculations are more nearly equivalently converged if they have the same number of plane waves or the same maximum kinetic energy. In any event, we repeated the B_{12}(CCC) calculation with $(\mathbf{k}+\mathbf{G})_{\max}=43.946$ Ry and obtained an increase in the cohesive energy of only 0.003 eV per unit cell.

[1]J. L. Hoard and R. E. Hughes, in *The Chemistry of Boron and Its Compounds,* edited by E. L. Muetterties (Wiley, New York, 1967), p. 25.

[2]*CRC Handbook of Chemistry and Physics* (CRC, Boca Raton, 1989), Vol. 70, (a) p. F19 and (b) p. D55.

[3]D. Emin, Phys. Rev. B **38**, 6041 (1988).

[4]A. C. Larson, in *Boron-Rich Solids (University of New Mexico Albuquerque, New Mexico),* Proceedings of an International Conference on the Physics and Chemistry of Boron and Boron-Rich Borides, AIP Conf. Proc. No. 140, edited by D. Emin, T. Aselage, C. L. Beckel, I. A. Howard, and C. Wood (AIP, New York, 1985), p. 109.

[5]A. Kirfel, A. Gupta, and G. Will, Acta. Crystallogr., Sect. B **35**, 1052 (1979).

[6]C. Wood and D. Emin, Phys. Rev. B **29**, 4582 (1984).

[7]D. R. Tallant, T. L. Aselage, A. N. Campbell, and E. Emin, Phys. Rev. B **40**, 5649 (1989).

[8]H. C. Longuet-Higgins and M. de V. Roberts, Proc. R. Soc. London, Ser. A **230**, 110 (1955).

[9]D. W. Bullett, J. Phys. C **15**, 415 (1982).

[10]M. van Schilfgaard and W. A. Harrison, J. Phys. Chem. Solids **46**, 1093 (1985).

[11]L. Kleinman and D. M. Bylander, Phys. Rev. Lett. **48**, 1425 (1982).

[12]E. L. Shirley, D. C. Allan, R. M. Martin, and J. D. Joannopoulos, Phys. Rev. B **40**, 3652 (1989).

[13]D. M. Bylander and L. Kleinman, Phys. Rev. B **41**, 907 (1990).

[14]W. Kohn and L. J. Sham, Phys. Rev. **104**, A1133 (1965).

[15]E. Wigner, Phys. Rev. **46**, 1002 (1934).

[16]A. Baldereschi, Phys. Rev. B **7**, 5212 (1973); D. J. Chadi and M. L. Cohen, *ibid.* **8**, 5747 (1973).

[17]M. Tinkham, *Group Theory and Quantum Mechanics* (McGraw-Hill, New York, 1964), p. 61.

[18]Perhaps $-kT\ln 5$ is closer to correct since it is unlikely that it would be energetically allowed to have both ends of an mteri-cosahedral bond occupied by carbon atoms.

[19]J. R. Chelikowsky and S. G. Louie, Phys. Rev. B **29**, 3470 (1984).

[20]B. K. Bhattacharyya, D. M. Bylander, and L. Kleinman, Phys. Rev. B **31**, 2049 (1985).

[21]C. Kittel, *Introduction to Solid State Physics,* 6th ed. (Wiley, New York, 1986), p. 55.

[22]B. K. Bhattacharyya, D. M. Bylander, and L. Kleinman, Phys. Rev. B **32**, 7973 (1985).

[23]Comparing the carbon fourfold and boron threefold ionization energies with E_C and E_B we find their errors to be $\Delta E_C=-1.728$ eV and $\Delta E_B=-1.015$ eV.

[24]J. C. Slater, *Symmetry and Energy Bands in Crystals* (Dover, New York, 1965), p. 418.

[25]Because of distortions away from rhombohedral symmetry, we do not pass through the center of this atom. This position of the unit cell has been chosen so that atom *B* is at its exact center.

[26]We centered the sphere midway between the *d* and *w* atoms on opposite sides of the icosahedron and took its radius to be $\frac{1}{2}(dw+dK)$.

[27]M. P. Teter, M. C. Payne, and D. C. Allan, Phys. Rev. B **40**, 12 255 (1989).

[28]D. M. Wood and A. Zunger, J. Phys. A **18**, 1343 (1985).

[29]W. H. Press, B. P. Flannery, S. A. Teukolsky, and W. T. Vetterling, *Numerical Recipes, The Art of Scientific Computing* (Cambridge University Press, Cambridge, England, 1986).

[30]G. H. Golub and C. F. van Loan, *Matrix Computations* (Johns Hopkins University Press, Baltimore, 1983), Sec. 10.3

[31]S. Lee, D. M. Bylander, and L. Kleinman, Phys. Rev. B **40**, 8399 (1989).

[32]M. T. Yin and M. L. Cohen, Phys. Rev. B **26**, 3259 (1982).

[33]O. H. Nielsen and Richard M. Martin, Phys. Rev. B **32**, 3792 (1985). Note the sign mistake in the first term of Eq. (2).

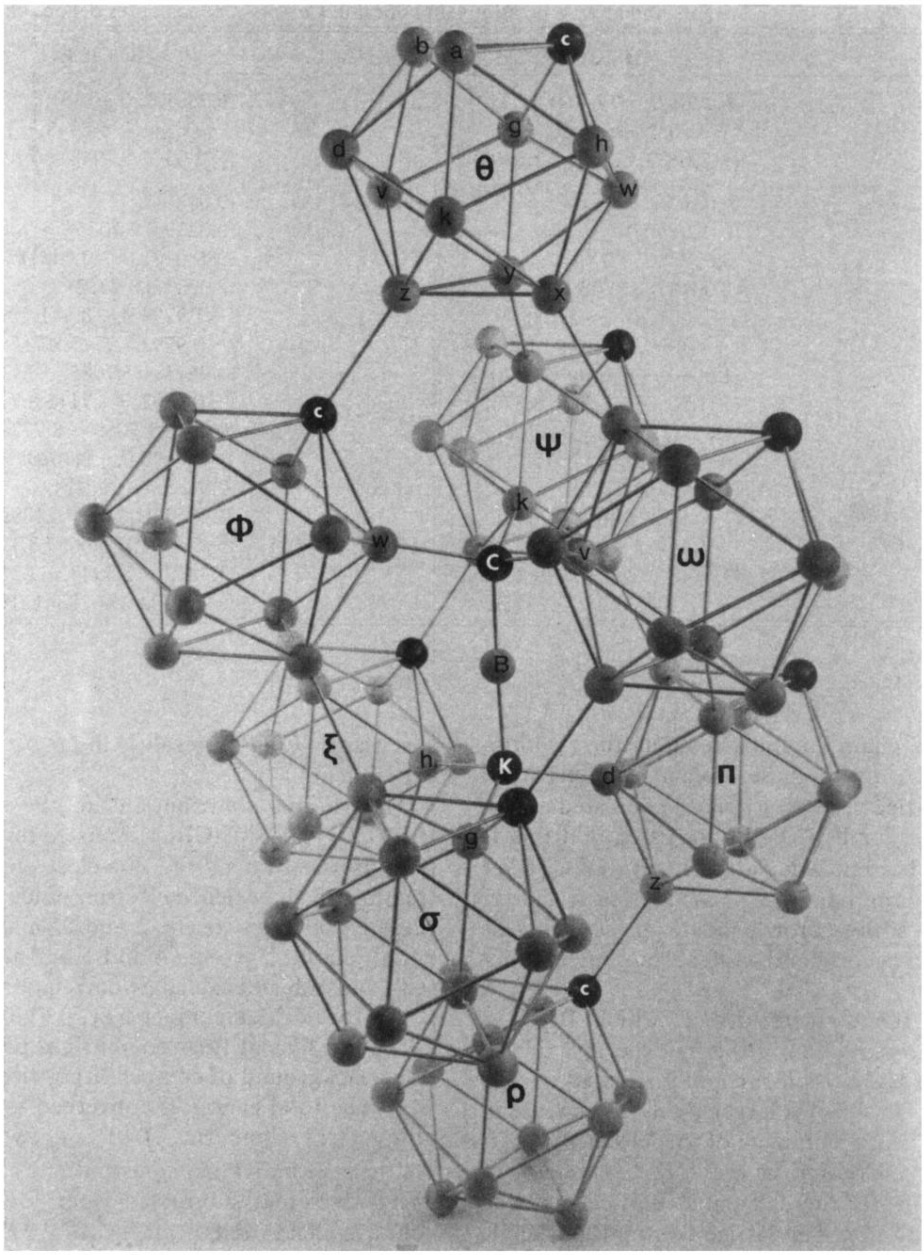

FIG. 1. Photograph of a $B_{11}C(CBC)$ crystal model, atoms *c*, *C*, and *K* are carbon and the rest are boron. Various lattice points in the middles of the icosahedra are labeled with Greek letters.